INTERANNUAL AND INTRASEASONAL VARIABILITIES OF THE FREE TROPOSPHERIC HUMIDITY USING METEOSAT WATER VAPOR CHANNEL OVER THE TROPICS

Hélène Brogniez, Rémy Roca and Laurence Picon
LMD/IPSL, Ecole Polytechnique, 91128 Palaiseau, France

ABSTRACT

Defined using the local humidity jacobian as a vertical averaging operator of the relative humidity over the free troposphere, the Free Tropospheric Humidity (FTH) is retrieved from METEOSAT Water Vapor cloud-cleared measurements. The resolution of the database in 0.625°x0.625° every 3 hours and allows documenting the variability of water vapor over Africa and the Atlantic Ocean from decadal to synoptic timescales. The analysis of the Eastern Mediterranean area reveals an interannual variability consistent with HIRS-12 observations. Thanks to the daily resolution of the new database, the intraseasonal variabilities of two summers of the 14 years period are then characterized. Using back-trajectories, these variabilities are further shown to be associated with extra-tropical/tropical large scale dynamical interactions.

1. Introduction

Water vapor is known to be a fundamental component of the Earth radiative budget. Thus, the study of its transport and distribution, at a wide range of space and time scales, will improve our knowledge of its role in the climate system. It has been highlighted that the clear sky outgoing longwave radiation is more sensitive to a humidity change in a dry environment [e.g. *Spencer and Braswell*, 1997]. The dry subsidence areas are then the most important source of infrared thermal energy loss. Measurements of so-called "Water Vapor" (WV) instruments provide observations of the water vapor of a thick layer of the troposphere. These WV data can be interpreted via a more geophysical variable which is the mean relative humidity of the free troposphere, generally named as the upper tropospheric humidity (UTH). The humidity retrieval has been applied during the last decade to WV instruments onboard several platforms such as GOES-7 [*Soden and Bretherton*, 1993], HIRS-12 on TOVS [*Stephens et al.*, 1996; *Soden and Bretherton*, 1996], or SSM/T-2 [*Spencer and Braswell*, 1997; *Engelen and Stephens*, 1998]. Since 1977, the successive METEOSAT geostationary satellites offer WV observations over Africa and the tropical Atlantic region, with high spatial and temporal resolutions [e.g. *Schmetz and Turpeinen*, 1988].

In this work, we first describe the Free Tropospheric Humidity (FTH) retrieval algorithm, based on a jacobian weighted relative humidity. Then, a 1983-1997 long-term archive of homogeneous METEOSAT-5 WV brightness temperatures developed at the LMD [see *Picon et al.*, 2003] is combined to an ISCCP-DX cloud-clearing methodology in order to retrieve FTH from both clear sky and low-level cloud pixels. Finally, this high spatial and temporal resolution database is used to study the driest area of the METEOSAT region, namely the Eastern Mediterranean. The FTH of this zone is analyzed at interannual and intraseasonal timescales. The moistest and driest boreal summers of the period are further analyzed using back-trajectories.

2. Free Tropospheric Humidity retrieval from METEOSAT WV measurements

a) Interpretation of WV data

Using a simplified radiative theory applied on an idealized thermodynamic profile and following empirical results [e.g. *Schmetz and Turpeinen*, 1988], *Soden and Bretherton* [1993] established an analytic

relationship between the mean relative humidity of a broad layer of the troposphere and the WV brightness temperature (T_{wv}):

$$aT_{wv} + b = \ln\left(\frac{\langle RH\rangle p_0}{\cos\theta}\right) \qquad (1)$$

where p_0 is a scaled reference pressure, p_0=p(T=T_{wv})/300 hPa; ‹*RH*› is the vertical average of the relative humidity *RH* (often referred as UTH); θ is the satellite viewing angle and *a* and *b* are fitting parameters. p_0 is a thermal parameter of the upper troposphere, and is determined assuming a mean T_{wv} of 240K. The vertical integration of ‹*RH*› can be performed by using either the weighting function derived from the transmission function [*Stephens et al.*, 1996], or by using weights defined from the sensitivity of the T_{wv} to small changes in a mean relative humidity profile [*Soden and Bretherton*, 1996] (hereafter SB96 weights or function). The SB96 function is, by definition, a relative humidity jacobian computed for a mean standard profile:

$$J_{RH} = \frac{\partial T_{wv}}{\partial RH} \qquad (2)$$

In this study, we introduce the *local* relative humidity jacobian function J_{RH} as a vertical averaging operator computed for each couple of temperature and humidity profiles. In the following, the relative humidity profiles are computed with respect to water only.

Figure 1 illustrates the 3 vertical averaging operators for 3 tropical atmospheres observed at nadir. Because the transmission derived weighting function is strongly affected by the absorber (i.e. H_2O molecule) concentration, the width of the function depends on the underlying moist layers. Therefore, in a dry free troposphere (warm T_{wv}), the weighting function will be influenced by the boundary layer and will peaks lower than the other functions (Fig 1 (c)). The humidity jacobian depend on both the transmission (absorber amount) and the temperature profile [*Jackson and Bates*, 2001]. However, the SB96 weights have been computed once for a standard profile: the transmission influence is therefore the one of the standard profile, and does not reflect locally the vertical absorber distribution. Moreover, the SB96 weights are expressed as a function of the temperature profile. Because over the METEOSAT area the temperature profiles are nearly constant, the maxima of the SB96 functions are constant at 350hPa in each of the 3 samples of the tropical and subtropical atmosphere (Fig 1 (a), (b) and (c)). The humidity jacobian J_{RH} computed locally using the radiative transfer model allows taking into account such a vertical variability of the absorber distribution. This is illustrated by Fig 1 (a) and (c), respectively the moist and the dry cases. Indeed, in the moist case, the J_{RH} function peaks at 300hPa, whereas in the dry case, the function peaks 150hPa below.

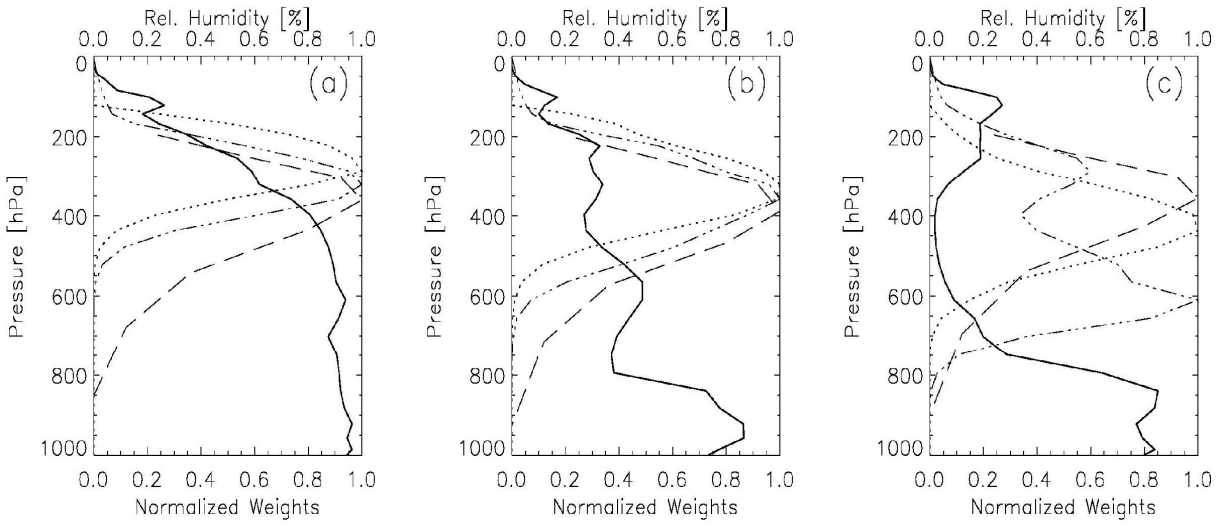

Fig 1: Vertical averaging operators for a moist case (a), an intermediate case (b), and a dry case (c). Weighting function is the mixed line, the SB96 function is the dashed line, and the J_{RH} function is the dotted line. The thick line is for the relative humidity profile.

In the tropics, and to be consistent with the observed widths of the weighted column (by any of the 3 weighting approaches) which mainly covers the free troposphere (Fig 1), the vertically weighted relative humidity ‹*RH*› of Eq (1) will be referred in the following as the Free Tropospheric Humidity (FTH).

b) Vertical averaging operator for METEOSAT WV measurements

The 3 averaging methods are then compared through the linear relationship of the retrieval algorithm (Eq (1)) on a sample of thermodynamic profile dataset located over the METEOSAT area, restricted to the tropical and subtropical belt [45°W-45°E/30°N-30°S]. This representative training dataset is obtained from ERA40 re-analyses [*Simmons and Gibson*, 2000] for January 1st and July 1st of 1992. Moreover, scenes covered with high- or medium-level clouds are removed from the dataset, leaving 8404 tropical profiles for the evaluation. METEOSAT-5 radiance calculations at 6.3μm (T_{wv}) are produced using the RTTOV-7 model [*Matricardi et al.*, 2001] that also provides the humidity jacobian J_{RH}. The p_0 parameter is computed directly from the ERA40 temperature profiles, to get locally the thermal structure information, and the satellite viewing geometry (θ) is also taken into account. The FTH product is computed using the 3 methods of vertical integration over the whole 700-200hPa layer.

Figure 2 shows that each of the 3 methods gives good results in terms of correlation. However, these plots highlight better correlations for the SB96 and the J_{RH} weights, respectively -0.981 and -0.994 (resp. Fig 2(b) and (c)). The global scatter obtained with the transmission derived weighting function is better in the cool areas than for the warmest scenes (Fig 2 (a)). The root-mean-square (RMS) error is an estimate of the quality of the fit. The RMS error, and thus the quality of the fit, improves when using the local J_{RH} weights (from 0.14/0.13 to 0.08, Fig 2 (c)).

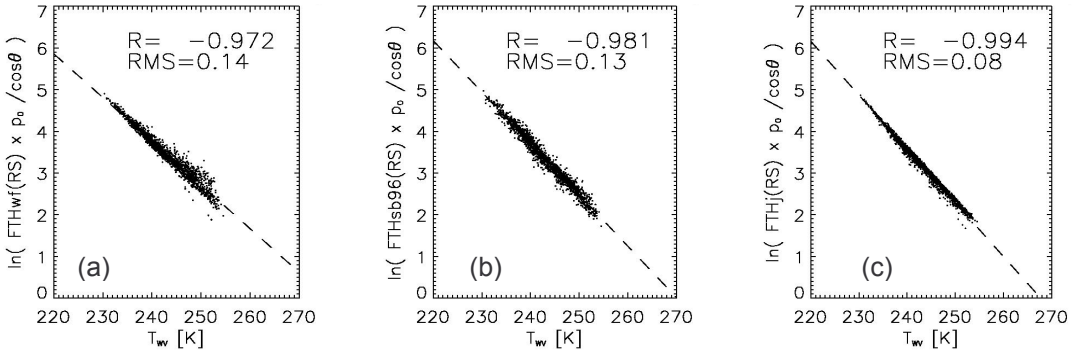

Fig 2: Scatter plots of synthetic radiance calculations T_{wv} versus the logarithmic relationship from eq (1). The FTH is computed using (a) the weighting function (FTH_{wf}), (b) the SB96 weights (FTH_{sb96}), and (c) the jacobian function (FTH_j).

Using the 3 fitting couples (*a*, *b)* obtained from each weighting method (Fig 2) and the local parameters p_0 and θ, the "retrieved" FTH of the training profiles are computed from Eq (1). The comparisons between the "observed" (weighted relative humidity profiles) and "retrieved" FTH are shown on Figure 3. The quality of the 3 products is then evaluated and the statistics of the retrievals are summarized on each plot (bias and root-mean-square error, in unit of *RH*). In order to evaluate the methods according to the dryness of the profile, the RMS error is computed in intervals of 5% of FTH and normalized with respect to the mean FTH of the bin (thick line in Fig 3).

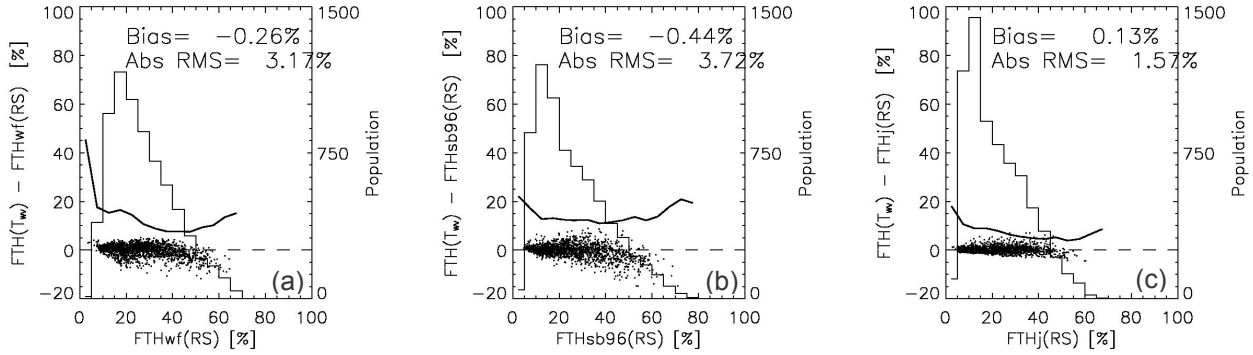

Fig 3: Scatter plots of the "observed" FTH from the 8404 ERA40 relative humidity profiles versus the bias between the "retrieved" FTH from T_{wv} and the "observed" FTH (see text) using (a) the weighting function, (b) the SB96 weights and (c) the J_{RH} function. The normalized RMS error (in %) is superimposed (thick line). The histogram is the "observed" FTH population.

The histograms of the "observed" FTH populations are also represented and show that either with the SB96 weights or with the J_{RH} function, the vertical averaging tends to produce more dry FTH (Fig 3 (b) and (c)). Indeed, the transmission derived weighting function tends to moisten the FTH (Fig 3(a)), as explained previously in § 2.a. Moreover, the scatter in the dry part of the plot is greater than with the other weighting methods: under 20% of FTH, the normalized RMS is about 16% (Fig 3(a)), whereas the normalized RMS is about 12% and 10% with the SB96 weights and the J_{RH} function respectively (Fig 3(b) and (c)). Considering the SB96 vertical averaging method, the normalized RMS is around 10-15% (Fig 3(b)) whereas the one of the improved method using the J_{RH} function is smaller than 10%, even 8% in the 25-50% range of the "observed" FTH. Finally, the best scatter and mean statistics are computed with the J_{RH} function leading to a mean bias of 0.13% and to a mean absolute RMS error of 1.57%.

The results of this evaluation lead us to define the METEOSAT-5 T_{wv} as a good surrogate of the relative humidity of the free troposphere (700-200hPa) weighted by the sensitivity function given by the humidity jacobian J_{RH}. The couple of fitting coefficients (a, b) obtained from Eq (1) with the J_{RH} function, are then used to retrieve the FTH of the whole METEOSAT-5 WV archive, spanning the 07/1983-02/1997 period.

3. Application to the nominal METEOSAT WV long-term archive

a) Low-level cloud effect on WV brightness temperatures and cloud-clearing methodology

Over cloudy area, the WV signal corresponds to the radiation at the top of the cloud, modulated by the underlying water vapor [e.g. *Schmetz and Turpeinen*, 1988]. The cloud impact on T_{wv} has been quantified under the grey body assumption for two synthetic dry profiles. The results show that for a FTH of 2%, a cloud at the 700hPa level cools the T_{wv} by 1.75K, whereas the radiative impact is less than 0.25K for a moister profile (FTH=20%). For these two cases, the absolute errors are small in terms of FTH: 0.45% for the driest profile and 0.65% for the moistest profile. Low-level clouds below the usual threshold of 700hPa have a small impact on the FTH retrieval and can thus be conserved for the cloud-clearing step. This result is consistent with the WV weighting function (derived from transmission, Fig 1 (b) or (c)) that suggest that low-level clouds at the top of the marine boundary layer, such as trade cumulus clouds, would be hardly detected by the WV radiometer.

Cloud information such as cloud top pressure is taken from the DX product level from the ISCCP database, at the spatial and temporal resolution of the B3 pixel level: 30km every 3 hours [e.g. *Rossow and Garder*, 1993]. The two maps on Figure 4 show the geographical results of the cloud-clearing for July 1992, using the 700hPa threshold on cloud top pressure. The main area concerned with this low-level cloud selection is the Atlantic Ocean. Indeed, in the Southern Atlantic, about 60% of the pixels kept in the monthly mean are low-level cloud scenes, likewise near the Azorean anticyclone were 30-35% of the pixels are associated to low-level cloud pixels (Fig 4(a)). Associated to these areas, a more or less strong warming of the T_{wv} is highlighted on Fig 4(b): this warming even reaches 2-2.5K in the Southern Atlantic. This observed warming could be induced by keeping low-level cloud scenes in the mean, such as strato-cumulus clouds, associated to strong subsidence [e.g. *Stevens et al.*, 2003] leading to a very dry free troposphere.

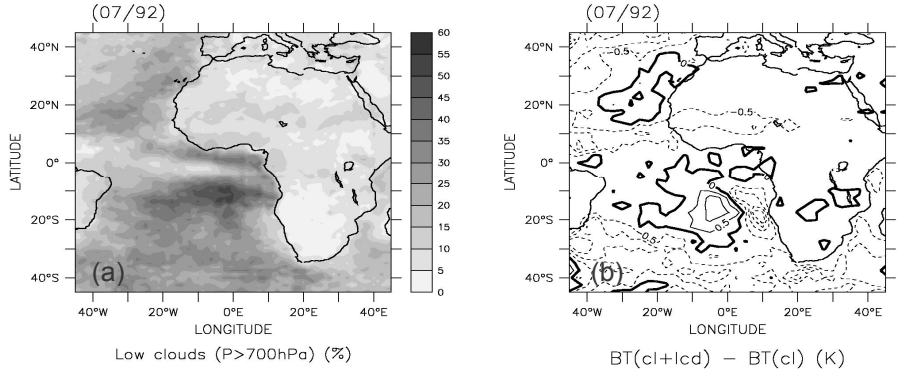

Fig 4: Maps for July 1992 (248 images) of (a) the percentage of low-level cloud pixels; (b) the difference between T_{wv} with clear and low-level clouds pixels and T_{wv} with only clear sky pixels. Dashed line is for negative differences; solid line is for positive differences.

Figure 4 not only shows the drying induced by the sampling of particular low-level clouds, but also the expected global cooling of keeping low-level clouds near convective systems. For example, over the ITCZ (around 0°N-15°N), the cloud-clearing increases the number of pixels kept in the monthly mean by 20-30% (Fig 4 (a)) and leads to a cooling of the T_{wv} by 0.5K. The ISCCP IR cloud detection is thus used to select pixels of both clear sky and low-level clouds (P_{top}≥700hPa), and the associated T_{wv} are kept for the FTH

retrieval. Note that the cirrus detection using only brightness temperatures (IR algorithm) needs to be improved [e.g. *Rossow and Garder*, 1993].

b) The long-term database: 07/1983 – 02/1997

The raw METEOSAT-2 to 5 T_{wv} have been recently reprocessed at the LMD to get a homogeneous long-term archive of METEOSAT-5 "equivalent" T_{wv}, giving the opportunity to make long-term coherent studies over Africa and tropical Atlantic [*Picon et al.*, 2003]. The cloud-cleared T_{wv} are then available on a regular grid of 0.625°, at the temporal resolution of 3 hours, from July 1983 until February 1997. Moreover, recent studies highlighted a warm bias of 2-3K in METEOSAT-5 and 7 brightness temperatures, due to a 10-15% bias in the calibration coefficient [e.g. *Köpken et al.*, 2003]. We thus performed a correction on the operational calibration with respect to the one of the HIRS-12 WV radiances using the methodology proposed by *Bréon et al.* [2000]. The adjustment of the calibration coefficient is applied on the radiances and leads to a change in T_{wv} of about 2.4K at 220K and 3.2K at 255K.

The global retrieval of FTH described in § 2 is then applied on the 14 years of METEOSAT-5 T_{wv} adjusted for the calibration bias, on clear and low-level cloud scenes. The interannual and the intraseasonal variabilities of the water vapor distribution can then be studied over Africa and the tropical/subtropical Atlantic Ocean. In the following, we focus on the particularly dry Eastern Mediterranean region.

4. Variability of the FTH in the Eastern Mediterranean area at interannual and intraseasonal scales

a) Interannual variability

Figure 5 represents the mean FTH of July-August (JA) over the period 1984-1996. The moist area associated to the ITCZ is evident with a FTH around 45-55%. On both side of the ITCZ, in the subtropics, strong and broad subsiding areas are present with a FTH lower than 10%. These two dry areas are of particular interest in terms of outgoing longwave radiation, and we focus here on the interannual and intraseasonal variabilities of the FTH over one of these two zones, namely the Eastern Mediterranean [27°E-37°E/27°N-35°N].

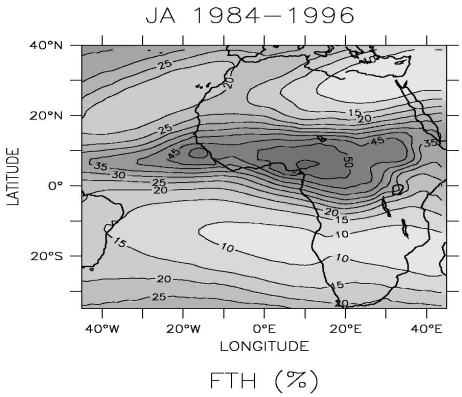

Fig 5: July-August mean of FTH for 1984-1996. The contour interval is 5%

First, the interannual variability of the METEOSAT-5 FTH product is compared over the Eastern Mediterranean to the HIRS-12 UTH product developed by *Jackson and Bates* [2001] and available on a 2.5° grid with a global coverage. The monthly means of the two products are illustrated on Figure 6, for the whole available period (July 1983 – February 1997).

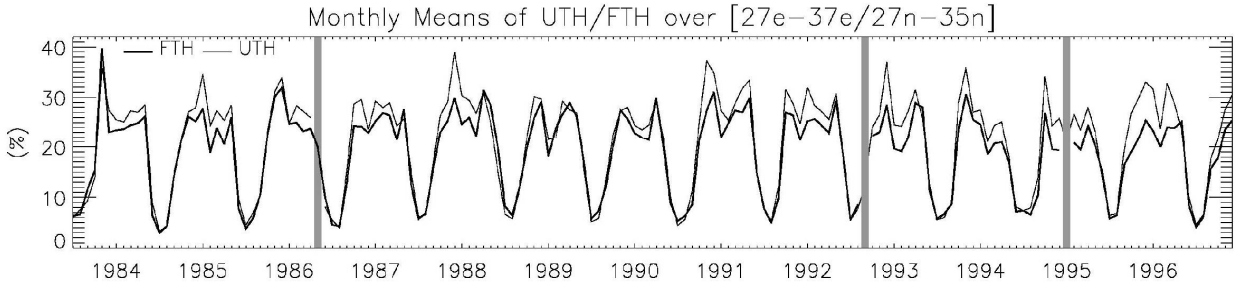

Fig 6: Monthly means of the UTH (thin line) and FTH (thick line) products over the Eastern Mediterranean are [27°E-37°E/27°N-35°N]. Major ticks indicate January. Gray zones represent missing data.

The results highlight a high temporal consistency between the two products, the UTH being slightly moister during the September-March season. A pronounced seasonal cycle is revealed over this area, a mean difference of about 25% being noticed between the winter and the summer seasons. Minima of F(U)TH are reached during July-August (JA): the driest summer occurs during JA 1984, whereas the moistest summers occur during JA 1992 and JA 1994.

b) Intraseasonal variability

Thanks to the high temporal resolution of the FTH database, the intraseasonal variability of the July-August season can be analyzed for each of the 14 available years, over the same area. In this paper, we focus on both the driest JA 1984 and the moistest JA 1992. The intraseasonal time series of daily means of FTH for the two JA are represented on Figure 7. While during JA 1992 the FTH is included in the 5-15% interval and presents two regimes (Fig 7 (b)), the FTH of JA 1984 is never beyond 6% and is characterized by a steady dry regime (Fig 7 (a)).

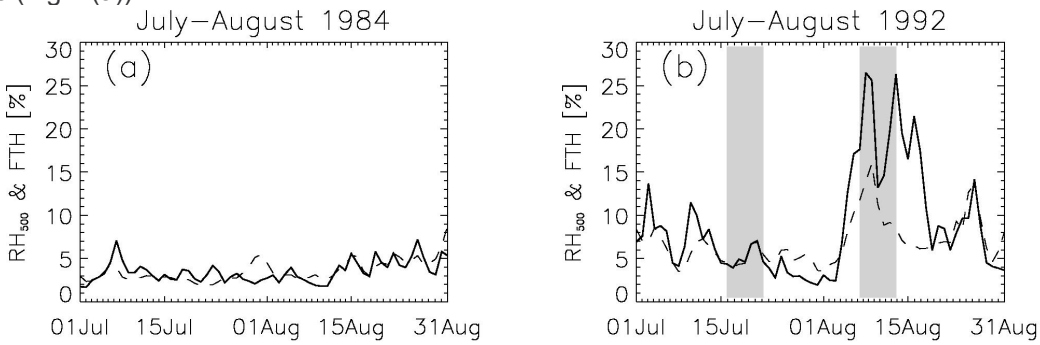

Fig 7: Daily means of the FTH (dashed line) over the Eastern Mediterranean area [27°E-37°E/27°N/35°N] for July-August 1984 (a) and 1992 (b). Gray zones on (b) delimit the 7-days phases (see text).

In order to deepen the analysis of the variability of these two summers, a back-trajectory model is first used to detail the interannual dynamic. The two regimes that occur during JA 1992 are also analyzed through two short phases of 7 days sufficiently separated in time: 16th to 22nd of July for the dry phase; 7th to 13th of August for the moist phase (Gray zones Fig 7 (b)).

c) Dynamical interpretation using back-trajectory results

The dynamical aspect of the FTH variability study is based on the assumption that the relative humidity field at 500hPa is taken as a good proxy of the FTH (see plain line on Fig 7 (a) and (b)). An advection/condensation Lagrangian model [*Pierrehumbert and Roca*, 1998] is used to determine the location of last saturation of air masses arriving at 500hPa over the considered area. The last saturation coordinates (i.e. latitude, longitude and pressure) are retrieved for each JA period (1984 and 1992) and are illustrated with zonally integrated latitude-pressure representations on Figure 8.

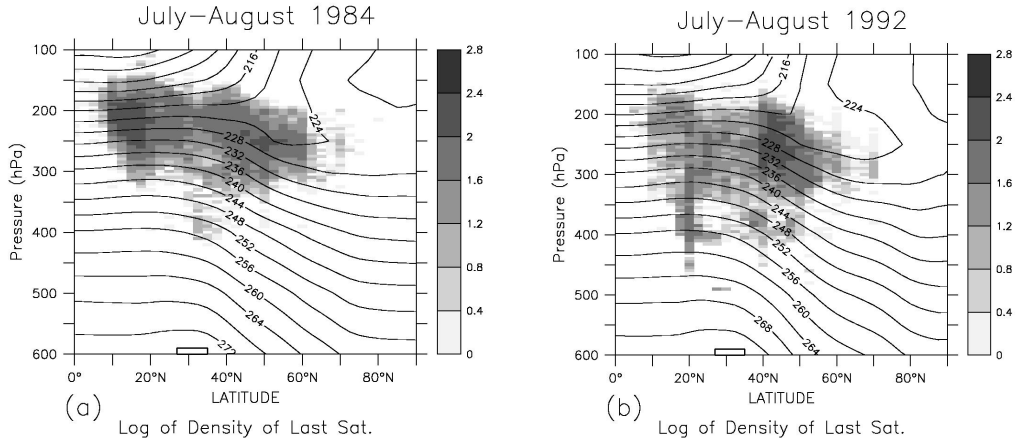

Fig 8: Zonally integrated distributions (in log scale) of air mass last saturations positions for July-August 1984 (a) and for July-August 1992 (b). Contours are for mean zonal air temperature over [80°W-80°E].

During the two periods, the air masses arriving over the Eastern Mediterranean have saturated at both tropical (10°N-20°N) and extra-tropical (40°N-60°N) latitudes (Fig 8). However, differences in the pressure of the last saturation are highlighted. In JA 1984 (Fig 8 (a)) the vertical density shows last saturation positions that are mainly located in the upper levels of the troposphere, between 275 and 150hPa, in a cold environment (232-214K). Considering JA 1992 (Fig 8 (b)), while the extra-tropical origins (>40°N) are mainly located in the upper troposphere (300-200hPa) at cold temperatures (236-224K), the tropical last saturations are located both in the upper levels and in the middle levels of the troposphere (400-150hPa) with environmental air temperature between 256 and 216K.

In the Lagrangian model used in this study, the humidity at the level of arrival (500hPa) is assumed to be linked to the saturated humidity of the coldest point encountered along the back-trajectory. The knowledge of the air temperature of the last saturation position is therefore a surrogate of the relative humidity at the level of arrival. The warmer is this last saturation point, the moister is the air mass arriving in the studied area. These thermodynamic assumptions are thus used to deepen the analysis for JA 1992. The density of air masses origins of the two 7-days phases described in the previous paragraph (Fig 7 (b)) are represented Figure 9.

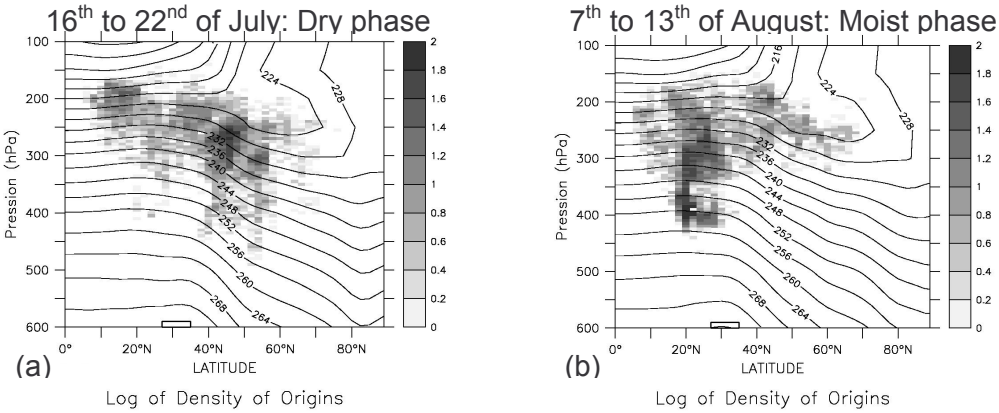

Fig 9: Zonally integrated distributions (in log scale) of air mass last saturations positions for the dry phase (a) and the moist phase (b) of July-August 1992. Contours are for the mean zonal air temperature over [80°W-80°E].

The dry phase (Fig 9 (a)) presents similar characteristics than July-August 1984 in terms of level (300-200hPa) and temperature (236-220K) of the last saturation positions which lead to a dry *RH* at the 500hPa level. The zonal integrations of the distributions highlight mainly extra-tropical origins (>40°N). The moist phase on Fig 9 (b) shows that during this period, the air masses found their origins in the middle tropical troposphere, around 400-300hPa, in a warmer environment (256-238K). Therefore the *RH* at the 500hPa level is moister compared to the drier periods.

At an interannual scale and over the Eastern Mediterranean, back-trajectory analyses reveal tropical/extra-tropical origins for the driest and the moistest summers of the 14 years, respectively July-August 1984 and 1992. The analysis of the intraseasonal variabilities of these two summers shows that during July-August 1992, the dry regime is characterized by extra-tropical air masses origins, similar to the overall dry JA 1984. The moist regime of this summer is mainly influenced by tropical air masses coming from warm levels of the middle troposphere. Part of theses tropical/extra-tropical air mass mixing has been recently highlighted with the MINOS campaign concerning pollutants transport over the Mediterranean [e.g. *Lelieveld et al*., 2002].

5. Concluding remarks

The cloud-cleared and homogeneous METEOSAT WV data, spanning 1983-1996, is used to study a long-term climatology of the Free Tropospheric Humidity over Africa and the tropical Atlantic region. The FTH is retrieved from T_{wv} using a global methodology and is defined from the relative humidity profile weighted by the water vapor jacobian function. The interannual climatology of the Eastern Mediterranean area show a pronounced seasonal cycle and a good consistency with the HIRS-12 retrieved UTH climatology. At an intraseasonal scale, the analysis of the driest and the moister July-August seasons of the 14 years highlight a tropical and extra-tropical air mass mixing having last saturated in high/low (cold/warm) levels associated to a dry/moist of the free troposphere of the area of arrival. The variabilities of the FTH over other key

regions of the METEOSAT area, such as the Southern Atlantic dry region or the moist Sahelian region, have also been studied.
This long-term climatology has been used to evaluate the water vapor distribution simulated by atmospheric general circulation model in the framework of the AMIP-2 project [*Brogniez et al.*, 2002].

Considering the retrieval of FTH, WV measurements from MSG would provide finer scale product that could be used to study small structures such as the environment of monsoonal convective systems, or dry air intrusion. Moreover, a local approach of the FTH algorithm is currently under study at the LMD. This approach is inspired from the operational UTH algorithm of Eumetsat based on local linear approximations of Eq (1) [e.g. *Schmetz et al.*, 1995] and needs further investigations.

6. References

Bréon F-M, D. Jackson and J. Bates (2000): *Calibration of the METEOSAT water vapor channel using collocated NOAA/HIRS-12 measurements*. J. of Geoph. Res., **105**, pp. 11,925-11,933.
Brogniez H., R. Roca and L. Picon (2002): *First results of the comparisons between METEOSAT Water Vapor data and some AMIP-II models.* Proceeding of the AMIP Workshop: towards innovative Model Diagnostics, Toulouse, France. Report of the World Climate Research Program.
Engelen R. and G. Stephens (1998): Comparison between TOVS/HIRS and SSM/T-2 derived upper tropospheric humidity. Bull. of the Am. Meteor. Soc., **78**, pp. 2748-2751.
Jackson D. and J. Bates (2001): *Upper Tropospheric humidity algorithm assessment*. J. of Geoph. Res., **106**, pp; 32,259-32,270.
Köpken C., J-N Thépaut and G. Kelly (2003): *Assimilation of geostationary WV radiances from GOES and METEOSAT at ECMWF*. EUMETSAT/ECMWF Fellowship Program, Res. Report n° 14.
Lelieveld J. and co-authors (2002): *Global air pollution crossroads over the Mediterranean*. Science, **298**, pp. 794-799.
Matricardi M., F. Chevallier, and S. Tjemkes (2001): *An improved general fast radiative transfer model for the assimilation of radiance observations*. ECMWF, Tech. Memo. n°345.
Picon L., R. Roca, S. Serrar, J-L Monge and M. Desbois (2003): *A new METEOSAT "water vapor" archive for climate studies*. J. of Geoph. Res., **108**, 4301, doi: 10.1029/2002JD002640.
Pierrehumbert R. and R. Roca (1998): *Evidence for control of Atlantic subtropical humidity by large scale advection*. Geoph. Res. Letters, **24**, pp. 4537-4540.
Rossow W. and L. Garder (1993): *Validation of the ISCCP cloud detection*. J. of Climate, **6**, pp. 2370-2393.
Schmetz J. and O. Turpeinen (1988): *Estimation of the upper tropospheric relative humidity field from METEOSAT water vapor image data.* J. of Appl. Meteor., **27**, pp. 889-899.
Schmetz J. and co-authors (1995): *Satellite observations of upper tropospheric relative humidity, clouds and wind field divergence*. Beitr. Phys. Atmos., **68**, pp. 345-357.
Simmons A. and J. Gibson (2000): *The ERA40 project plan.* ERA-40 Project, Report Series n°1.
Soden B. and F. Bretherton (1993): *Upper tropospheric relative humidity from the GOES 6.7μm channel: method and climatology for July 1987*. J. of Geoph. Res., **98**, pp. 16,669-16,688.
Soden B. and F. Bretherton (1996): *Interpretation of TOVS water vapor radiances in terms of layer-average relative humidities: method and climatology for the upper, middle, and lower troposphere*. J. of Geoph. Res., **101**, pp. 9333-9343.
Spencer and Braswell (1997): *How dry is the tropical free troposphere? Implications for global warming theory.* Bull. of the Am. Meteor. Society, **78**, pp. 1097-1106.
Stephens G., D. Jackson and I. Wittmeyer (1996): *Global observations of upper tropospheric water vapor derived from TOVS radiance data*. J. of Climate, **9**, pp. 305-326.
Stevens and co-authors (2003): *Dynamics and chemistry of marine stratocumulus-DYCOMS-II*. Bull. of the Am. Meteor. Soc., **84**, pp. 579–593.